Photoelectron Spectroscopy and ab Initio Study of B_3^- and B_4^- Anions and Their Neutrals

Hua-Jin Zhai and Lai-Sheng Wang*

Department of Physics, Washington State University, 2710 University Drive, Richland, Washington 99352, and W. R. Wiley Environmental Molecular Sciences Laboratory, Pacific Northwest National Laboratory, MS K8-88, P.O. Box 999, Richland, Washington 99352

Anastassia N. Alexandrova and Alexander I. Boldyrev*

Department of Chemistry and Biochemistry, Utah State University, 0300 Old Main Hill, Logan, Utah 84322-0300

Vyacheslav G. Zakrzewski

Department of Chemistry, Kansas State University, 111 Willard Hall, Manhattan, Kansas 66506-3701

Received: June 16, 2003; In Final Form: August 21, 2003

The two smallest boron clusters (B_3 and B_4) in their neutral and anionic forms were studied by photoelectron spectroscopy and ab initio calculations. Vibrationally resolved photoelectron spectra were observed for B_3^- at three photon energies (355, 266, and 193 nm), and the electron affinity of B_3 was measured to be 2.82 ± 0.02 eV. An unusually intense peak due to two-electron transitions was observed in the 193-nm spectrum of B_3^- at 4.55 eV and its origin was theoretically characterized. We confirmed that both B_3^- and B_3 are π and σ aromatic systems with D_{3h} symmetry. The photoelectron spectra of B_4^- were also obtained at the three photon energies, but much broader spectra were observed. The B_4^- anion was found to have the lowest electron detachment energy (~1.6 eV) among all boron clusters with three or more atoms, consistent with its extremely weak mass signals. The neutral B_4 cluster was found to have a D_{2h} rhombus structure, which is only slightly distorted from a perfect square. For B_4^-, we identified computationally two low-lying isomers ($^2B_{1u}$ and ^2A_g) both with D_{2h} symmetry, with the $^2B_{1u}$ state slightly more stable, which is confirmed through comparison of the calculated spectra with the experimental spectra. The chemical bonding of the two small boron clusters is discussed in terms of aromaticity and antiaromaticity both in the π and σ frameworks. We demonstrated that the aromaticity and antiaromaticity concepts provide us a clear explanation of the chemical structure and bonding in these two boron clusters.

1. Introduction

Boron clusters represent the lightest covalently bound species and understanding the electronic and atomic structures in these systems is important for the development of a unified chemical bonding theory for all covalently bound molecules. Small clusters frequently adopt a different structure from being just small pieces of the corresponding bulk materials. Therefore, chemical bonding theories, which can successfully explain the structures and stabilities of bulk crystals, may not provide us with similar explanations in clusters. Boron clusters present the best testimony to this expectation. Although bulk boron in its numerous modifications consists of networks of icosahedral units covalently bound to each other,[1,2] small boron clusters adopt planar or quasiplanar structures.[3−46] However, even though boron clusters have been the subjects of numerous theoretical[3−38] and experimental[39−45] studies, the electronic structure and chemical bonding in such species did not receive much attention until recently.[25−27,31−38] Furthermore, the structures of many small boron clusters considered computationally were not verified experimentally. In a series of recent articles, we have reported joint experimental and theoretical studies of a number of boron clusters, B_5^-,[35] B_6^-,[36] B_8^- and B_9^-,[37] B_{10}^-−B_{15}^-,[38] and their neutrals. The structures of these clusters were searched computationally and verified through comparisons of experimental and theoretical photoelectron spectra. We have confirmed the two-dimensional nature of all these clusters, and in particular, we have shown that the concepts of aromaticity and antiaromaticity can be successfully used for explaining their structures and stability.

However, the smallest B_3^- and B_4^- clusters have escaped our initial experimental detection and their photoelectron spectra have been only obtained recently. In the meantime, some of us (A.E.K. and A.I.B.) have reported a theoretical analysis of B_3^-.[46] A theoretical study of B_4^- has also appeared recently.[34] In the current paper, we report the photoelectron spectra of B_3^- and B_4^- and compare them with an accompanying theoretical study. Very sharp and vibrationally resolved spectra were obtained for B_3^-. Interestingly, our theoretical analyses revealed an unusual two-electron transition present in the photoelectron spectra, suggesting strong electron correlation effects in B_3^-. The spectra of B_4^- on the other hand were broad and no vibrational structures were observed in the threshold band, indicating a large geometry change from B_4^- to B_4 neutral. Our theoretical analysis showed that B_4^- has D_{2h} symmetry with a $^2B_{1u}$ ground state, with a low-lying ^2A_g state. Neutral B_4 was also shown to have D_{2h} symmetry with a ^1A_g ground state. A large bond angle

* To whom correspondence should be addressed. E-mail: ls.wang@pnl.gov. E-mail: boldyrev@cc.usu.edu.

10.1021/jp0357119 CCC: $25.00
Published on Web 10/10/2003

change was observed between the ground states of the anion and neutral B_4, consistent with the broad photoelectron spectra.

2. Experimental Methods

The experiment was carried out using a magnetic-bottle time-of-flight photoelectron apparatus equipped with a laser vaporization supersonic cluster source.[47,48] The B_3^- and B_4^- anions were produced by laser vaporization of a disk target made of enriched ^{10}B isotope (99.75%) in the presence of a helium carrier gas. Various clusters were produced from the cluster source and were analyzed using a time-of-flight mass spectrometer. The cluster species of interest (B_3^- or B_4^-) were mass-selected and decelerated before being photodetached. Three detachment photon energies were used in the current experiments: 355 (3.496 eV), 266 (4.661 eV), and 193 nm (6.424 eV). Photoelectron spectra were calibrated using the known spectrum of Rh^-, and the resolution of the apparatus was better than 30 meV for 1 eV electrons.

Although B_3^- and B_4^- are the smallest and simplest boron clusters, the photodetachment experiment turned out to be rather challenging, primarily because of the weak cluster intensities and the low photodetachment cross sections of these light clusters. The timings of firing the vaporization laser, the helium carrier gas pulse, and the ion extraction all had to be controlled much more delicately to ensure sufficient mass signals for the photodetachment experiment. Even with the extreme cares taken, the mass intensities of B_3^- and B_4^- were still rather weak. This was especially true for B_4^-, which possesses the lowest electron affinity among all boron clusters B_n^- ($n = 3-25$) and appears to be "anti-magic" in the mass spectrum. Consequently, the B_4^- ion beam could not be decelerated sufficiently to achieve our best resolution in the photoelectron experiment, and a much longer averaging time (several hundred thousand laser shots) was needed to acquire a spectrum with reasonable signal-to-noise ratios.

3. Theoretical Methods

An extensive search of the global minima structure of B_3, B_3^-, B_4, and B_4^- was performed using a hybrid method, which includes a mixture of Hartree−Fock (HF) exchange with density functional exchange-correlation potentials (B3LYP)[49−51] with the polarized split-valence basis sets (6-311+G*).[53,54] For the lowest energy structures, geometries were refined using the restricted coupled cluster method [RCCSD(T)][55−57] with the same basis set. We found that the unrestricted HF method and all post HF methods based on the unrestricted HF method have a very high spin-contamination. Therefore, results at these levels of theory may be unreliable. We further refined energies of the lowest isomers at the RCCSD(T) level of theory with an extended basis set (6-311+G(2df)). The CASSCF(8,12) calculations[58,59] for B_3^- and the CASSCF(9,12) calculations for B_4^- with the 6-311+G* basis set were performed to test the multiconfigurational nature of their wave functions. Also, multiconfigurational single-point calculations (CASSCF-MRCISD)[60,61] with the extended 6-311+G(2df) basis set and various active space and number of active electrons were used for additional investigation of the relative energies for the two lowest states of the B_4^- anion.

The theoretical photoelectron spectrum of B_3^- was calculated using the ADC(3)[62−66] and the RCCSD(T) methods with the 6-311+G(2df) basis set. Because B_4^- has a doublet ground state, two theoretical methods were employed to calculate its photoelectron spectrum. The RCCSD(T) methods with the 6-311+G(2df) basis set was used to calculate vertical electron detachment energies (VDEs) to the triplet final states and the equation of motion method based on the restricted coupled cluster method [EOM-CCSD(T)][67] with the 6-311+G(2df) basis sets was used to calculate the VDEs to the final singlet states. The first VDEs of the two lowest states of B_4^- were also evaluated as the VDEs to the singlet ground state of B_4 using the ROVGF[68−71] and ACD(3) methods with the 6-311+G(2df) basis sets and the optimal geometries for their respective anionic states obtained at the RCCSD(T)/6-311+G* level of theory. The chemical bonding in the boron trimer and tetramer was interpreted using molecular orbital pictures drawn at the U(R)HF/6-311+G* level of theory.

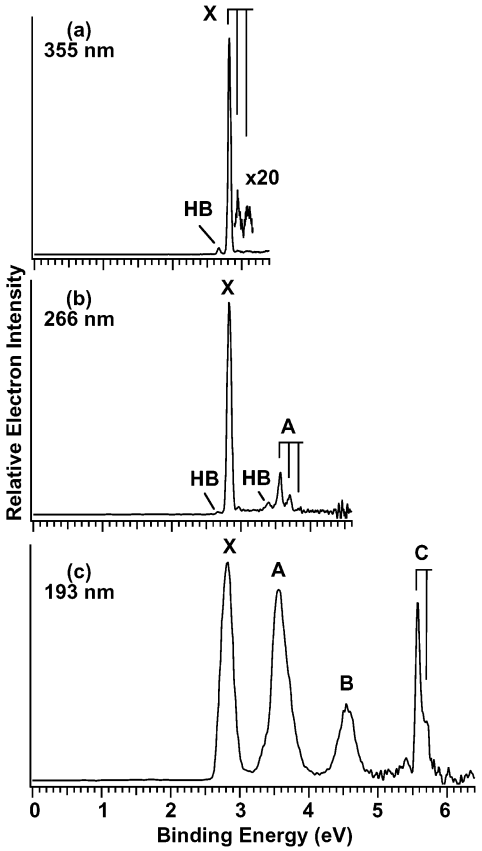

Figure 1. Photoelectron spectra of B_3^- at (a) 355 nm (3.496 eV), (b) 266 nm (4.661 eV), and (c) 193 nm (6.424 eV). HB stands for hot band transitions. The vertical lines indicate resolved vibrational structures.

B3LYP, ROVGF, CASSCF, and U(R)HF calculations were done using Gaussian 98.[72] The ACD(3) calculations were done using the program written by V. G. Zakrzewski and incorporated into Gaussian 98. RCCSD(T), EOM-RCCSD(T), and CASSCF-MRCI calculations were done using the MOLPRO 1999 program.[73] All molecular orbital pictures were drawn using the Molden 3.4 program.[74] Calculations were performed on a 63-nodes Birch-Retford Beowulf cluster computer built at Utah State University by K. A. Birch and B. P. Retford.

4. Experimental Results

4.1. Photoelectron Spectra of B_3^-. The photoelectron spectra of B_3^- are shown in Figure 1 at three photon energies. At 355 nm, a strong and sharp peak (X) was observed with a short vibrational progression and a hot band transition. The sharp peak defined the electron affinity (EA) of B_3 to be 2.82 ± 0.02 eV. The short vibrational progression and the hot band yielded vibrational frequencies for the ground states of the neutral and

TABLE 1: Observed Adiabatic (ADE) and Vertical (VDE) Detachment Energies and Vibrational Frequencies for B_3^- and B_4^-

observed band	ADE (eV)	VDE (eV)	vib. freq. (cm^{-1})
		B_3^- [a]	
X	2.82 ± 0.02	2.82 ± 0.02	1020 ± 50
A	3.56 ± 0.03	3.56 ± 0.03	1130 ± 40
B		4.55 ± 0.04	
C	5.58 ± 0.03	5.58 ± 0.03	1100 ± 80
		B_4^-	
X	~1.6	1.99 ± 0.05	
A		3.08 ± 0.03	690 ± 60
B		3.41 ± 0.03	
C		4.39 ± 0.05	

[a] A vibrational frequency of 1230 ± 40 cm^{-1} was determined for B_3^- from the observed hot band transitions (see Figure 1).

the anion of 1020 ± 50 and 1230 ± 40 cm^{-1}, respectively. At 266 nm, a weaker band (A) was observed, which also showed a short vibrational progression and a hot band. The A band represents the first exited state of B_3.

At 193 nm, two more bands (B and C) were observed. The relatively weak B band with a VDE of 4.55 eV seemed to show a strong photon energy dependence, because this band was not observable in the 266 nm spectrum (Figure 1b). The A band also showed a strong photon energy dependence, and its relative intensity was significantly enhanced in the 193 nm spectrum. The high binding energy band (C) was observed with a VDE of 5.58 eV, and it also showed a short vibrational progression. The observed ADEs, VDEs, and vibrational frequencies for B_3^- are given in Table 1.

4.2. Photoelectron Spectra of B_4^-. The spectra of B_4^- at the three photon energies are shown in Figure 2. Four very broad bands were observed. The A and B bands were closely spaced and were overlapped. At 355 nm, vibrational structures were discernible for the A band (Figure 2a). The broad X band indicated a large geometry change between the ground states of the anion and neutral B_4. The VDE of the X band was measured to be 1.99 ± 0.05 eV. However, the ADE was difficult to determine because of the width of the band and the lack of vibrational resolution. Considering the potential hot band transitions, we estimated the ADE or the EA of B_4 to be ~1.6 eV. This makes the EA of B_4 to be the lowest among all the boron clusters from B_3 to B_{25}, partly explaining why the B_4^- anion was relatively unstable and had the weakest abundance in our cluster source. The obtained ADEs, VDEs, and vibrational frequencies for B_4^- are also given in Table 1.

5. Theoretical Results

5.1. B_3 and B_3^-. An extensive search for the global minimum of B_3^- was performed previously.[46] It was found to have D_{3h} symmetry with a $^1A_1'$ electronic state ($1a_1'^2 1e'^4 1a_2''^2 2a_1'^2$), consistent with prior studies. An electron detachment from the HOMO ($2a_1'$) of B_3^- yields a D_{3h} structure with a $^2A_1'$ electronic state ($1a_1'^2 1e'^4 1a_2''^2 2a_1'^1$), which was found to be the global minimum for neutral B_3. These results agree with all previous theoretical[5,6,12] and experimental[44] data. The HF wave function was dominant in the CASSCF(7,12)/6-311+G* expansions for B_3 ($C_{HF} = 0.8926$ among the 108 900 configurations) and in the CASSCF(8,12)/6-311+G* for B_3^- ($C_{HF} = 0.9153$ among the 122 760 configurations), ensuring that the RCCSD(T) calculations were reliable. Therefore, the global minimum structures of B_3 and B_3^- were well-established computationally. The optimized geometries, total energies, and the calculated harmonic frequencies for B_3 and B_3^- are summarized in Table 2.

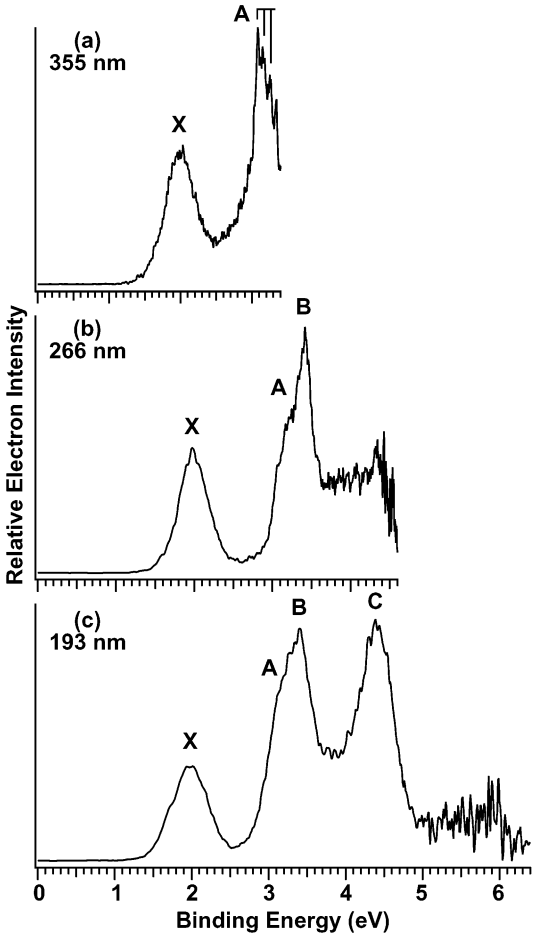

Figure 2. Photoelectron spectra of B_4^- species at (a) 355, (b) 266, and (c) 193 nm.

5.2. B_4 and B_4^-. Our search for the global minimum structures of B_4^- (Figure 3) and B_4 (Figure 4) at the B3LYP/6-311+G* level of theory revealed that both species have a rhombus structure (D_{2h} symmetry) with a $^2B_{1u}$ ($1a_g^2 1b_{1u}^2 1b_{2u}^2 b_{3u}^2 2a_g^2 1b_{3g}^2 2b_{1u}^1$) and a ^1A_g ($1a_g^2 1b_{1u}^2 1b_{2u}^2 b_{3u}^2\ 2a_g^2 1b_{3g}^2 2b_{1u}^0$) spectroscopic state, respectively. Our finding for the ground state of neutral B_4 (Table 3 and Figure 4) is consistent with previous ab initio calculations.[7,9,11,21,34] However, our ground electronic state for the B_4^- anion is different from a previously reported D_{2h} ^2A_g state ($1a_g^2 1b_{1u}^2 1b_{2u}^2 b_{3u}^2 2a_g^2 1b_{3g}^2 3a_g^1$).[34] At the B3LYP/6-311+G* level of theory, the D_{2h} ^2A_g state was found to be 6.1 kcal/mol higher in energy with a significantly larger ∠B1−B2−B3 angle (Table 4). When we re-optimized the geometries of the two B_4^- isomers at the RCCSD(T)/6-311+G* level of theory we found that the $^2B_{1u}$ state is higher in energy than the ^2A_g state by 2.04 kcal/mol. The RCCSD(T)/6-311+G(2df)//CCSD(T)/6-311+G* calculations reduced the energy difference to 0.4 kcal/mol with the $^2B_{1u}$ state still being higher in energy (Table 4). To test further which of these two states is lower in energy, we performed CASSCF(3,4)-MRCISD/6-311+G(2df) and CASSCF(3,5)-MRCISD/6-311+ G(2df) calculations. At these levels of theory, the $^2B_{1u}$ state is lower in energy than the ^2A_g state by 3.0 and 5.8 kcal/mol, respectively.

We further evaluated the relative energies of these two states through combined calculations at the RCCSD(T)/6-311+G(2df) and ROVGF/6-311+G(2df) or ACD(3)/6-311+G(2df) levels of theory. First, the total energy of the B_4 cluster was calculated at the RCCSD(T)/6-311+G(2df) level of theory using the

TABLE 2: Molecular Properties of B_3 and B_3^-

	B_3 D_{3h} ($^2A_1'$)			B_3^- D_{3h} ($^1A_1'$)			
	B3LYP/ 6-311+G*	RCCSD(T)/ 6-311+G*	RCCSD(T)/ 6-311+G(2df)// RCCSD(T)/6-311+G*	B3LYP/ 6-311+G*	RCCSD(T)/ 6-311+G*	RCCSD(T)/ 6-311+G(2df)// RCCSD(T)/6-311+G*	CASMRCI/ 6-311+G(2df)[b]
E_{total}, a.u.	−74.298272	−74.063356	−74.091367	−74.397068	−74.164651	−74.196742	−74.166109
R(B−B), Å	1.548	1.582	*a*	1.542	1.576	*a*	1.552
$\omega_1(a_1')$, cm^{-1}	1223	*a*	*a*	1239	1190	*a*	*a*
$\omega_2(e')$, cm^{-1}	934	*a*	*a*	959	897	*a*	*a*

[a] Properties were not calculated at this level of theory. [b] Active space for the CAS-MRCI was constructed the following way: rhf;occ,5,1,2,0;closed,5,1,2,0;core,2,0,1,0; wf,16,1,0;multi/ci;occ,8,1,4,0;closed,3,0,1,0;core,2,0,1,0;wf,16,1,0.

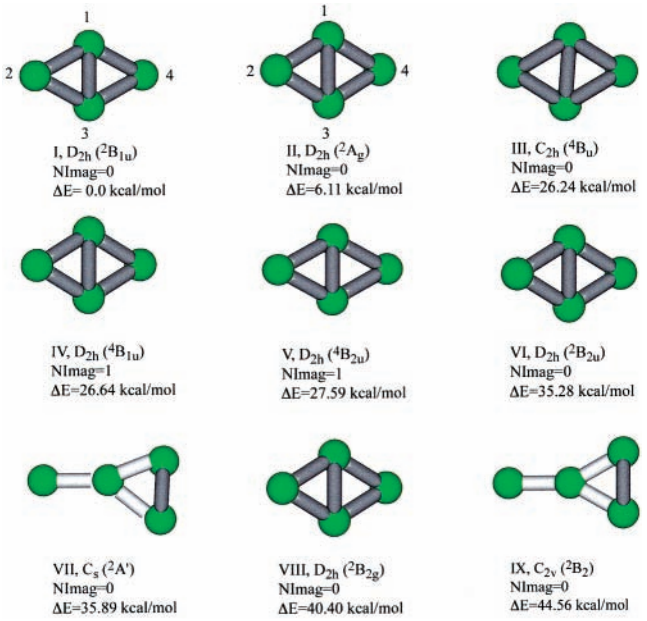

Figure 3. Optimized structures and their relative energies of B_4^- at B3LYP/6-311+G* level of theory.

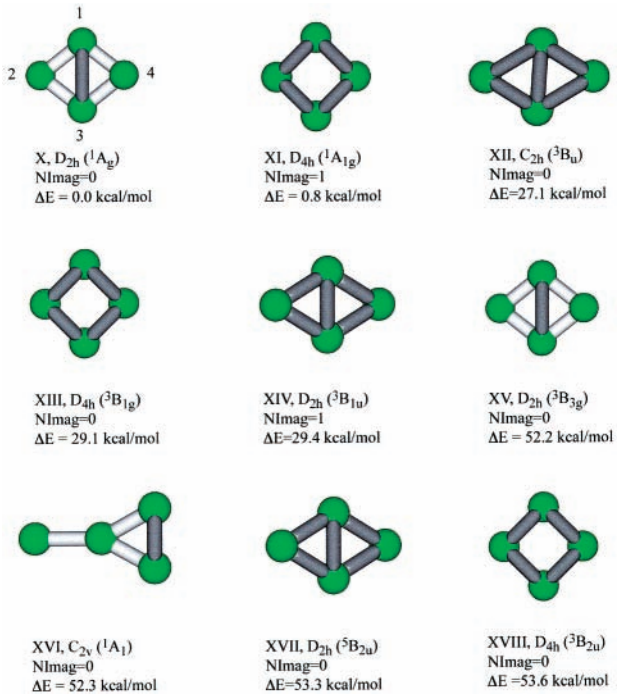

Figure 4. Optimized structures and their relative energies of B_4 at B3LYP/6-311+G* level of theory.

RCCSD(T)/6-311+G* optimal geometries of B_4^- at the $^2B_{1u}$ and ^2A_g states. Then, the vertical electron attachment energy was calculated at either ROVGF/6-311+G(2df) or ADC(3)/6-311+G(2df) leading to the $^2B_{1u}$ or to the ^2A_g states at their appropriate optimal geometries again at the RCCSD(T)/6-311+G* level of theory. Combining the total energies of the B_4 cluster at RCCSD(T)/6-311+G(2df) with the vertical electron attachment energies at either ROVGF/6-311+G(2df) or ADC-(3)/6-311+G(2df), we obtained the total energies of the two lowest anionic states. At the RCCSD(T)/6-311+G(2df)+ROVGF/6-311+G(2df) level of theory, the B_4^- ($^2B_{1u}$) state was found to be more stable than the B_4^- (^2A_g) state by 3.7 kcal/mol and at the RCCSD(T)/6-311+G(2df)+ADC(3)/6-311+G(2df) level of theory by 2.1 kcal/mol.

On the basis of all the above calculations, we conclude that the $^2B_{1u}$ state is more stable and is the ground state of the B_4^- anion. Other low-lying isomers for B_4^- are presented in Figure 3.

6. Interpretation of the Photoelectron Spectra of B_3^-

The VDEs of the B_3^- anion was calculated previously at the ROVGF/6-311+G(2df)//CCSD(T)/6-311+G* level of theorty.[46] In the current work, we further calculated the VDEs at two additional levels of theory: ACD(3)/6-311+G(2df) and RCCSD-(T)/6-311+G(2df). Our new theoretical results together with the previous ab initio calculations are summarized and compared with the experimental data in Table 5.

TABLE 3: Molecular Properties of B_4

	B3LYP/ 6-311+G*	RCCSD(T)/ 6-311+G*	RCCSD(T)/ 6-311+G(2df)// RCCSD(T)/6-311+G*
E_{total}, a.u.	−99.157546	−98.839444	−98.881103
R(B1−B2), Å	1.523 Å	1.558 Å	*a*
∠B1−B2−B3	76.5°	75.4°	*a*
$\omega_1(a_g)$, cm^{-1}	1183	1112	*a*
$\omega_2(a_g)$, cm^{-1}	332	336	*a*
$\omega_3(b_{3g})$, cm^{-1}	1268	1173	*a*
$\omega_4(b_{1u})$, cm^{-1}	1267	1201	*a*
$\omega_5(b_{2u})$, cm^{-1}	1059	966	*a*
$\omega_6(b_{3u})$, cm^{-1}	320	287	*a*

[a] Properties were not calculated at this level of theory.

6.1. X and A Bands. The X band corresponds to the detachment of an electron from the $2a_1'$-HOMO of B_3^-, which is depicted in Figure 5. The calculated VDE at all three levels of theory agrees well with the experimental data (Table 5). The RCCSD(T) value (2.88 eV) reproduces almost exactly the experimental VDE (2.82 ± 0.02 eV). Good agreement was also found between the theoretical ADE [2.87 eV at RCCSD(T)] and the experimental ADE (2.82 ± 0.02 eV). The $2a_1'$ HOMO is formed by the radial p_σ orbitals of the three boron atoms, and it is a complete bonding orbital. Electron detachment from this MO should not change the symmetry of the cluster, but might lead to a relaxation in the B−B bond lengths. The sharp

TABLE 4: Molecular Properties of B_4^-

	B_4^-, D_{2h} ($^2B_{1u}$)				B_4^-, D_{2h} (^2A_g)			
	B3LYP/ 6-311+G*	RCCSD(T)/ 6-311+G*	RCCSD(T)/ 6-311+G(2df)//RCCSD(T)/ 6-311+G*	CASSCF-MRCISD/[b] 6-311+G(2df)//RCCSD(T)/ 6-311+G*	B3LYP/ 6-311+G*	RCCSD(T)/ 6-311+G*	RCCSD(T)/ 6-311+G(2df)//RCCSD(T)/ 6-311+G*	CASSCF-MRCISD/[b] 6-311+G(2df)//RCCSD(T)/ 6-311+G*
E_{total}, a.u.	−99.226968	−98.895463	−98.940051	−98.948199	−99.217253	−98.898718	−98.940741	−98.943504
ΔE, kcal/mol	0.0	2.04	0.43	0.0	6.1	0.0	0.0	2.95
R(B1−B2), Å	1.568	1.595 Å	*a*	*a*	1.578 Å	1.621 Å	*a*	*a*
∠B1−B2−B3	63.5°	63.6°	*a*	*a*	84.3°	73.8°	*a*	*a*
$\omega_1(a_g)$, cm^{-1}	1138	*a*	*a*	*a*	1053	*a*	*a*	*a*
$\omega_2(a_g)$, cm^{-1}	800	*a*	*a*	*a*	136	*a*	*a*	*a*
$\omega_3(b_{3g})$, cm^{-1}	1039	*a*	*a*	*a*	1116	*a*	*a*	*a*
$\omega_4(b_{1u})$, cm^{-1}	1008	*a*	*a*	*a*	738	*a*	*a*	*a*
$\omega_5(b_{2u})$, cm^{-1}	804	*a*	*a*	*a*	844	*a*	*a*	*a*
$\omega_6(b_{3u})$, cm^{-1}	284	*a*	*a*	*a*	336	*a*	*a*	*a*

[a] Properties were not calculated at this level of theory. [b] Active space for the CAS-MRCI (3 by 4) calculations were chosen the following ways: isomer B_4^-, D_{2h} ($^2B_{1u}$): rhf;occ,4,1,2,0,3,0,1,0;closed,4,1,2,0,2,0,1,0;core,2,0,1,0,1,0,0,0;wf,21,5,1;multi/ci;occ,5,1,2,0,3,1,1,0;closed,3,1,2,0,1,0 ,1,0; core,2,0,1,0,1,0,0,0;wf,21,5,1; isomer B_4^-, D_{2h} (^2A_g): rhf;occ,5,1,2,0,2,0,1,0;closed,4,1,2,0,2,0,1,0;core,2,0,1,0,1,0,0,0;wf,21,1,1; multi/ci;occ, 5,1,3,0,3,0,1,0;closed,3,0,2,0,2,0,1,0;core,2,0,1,0,1,0,0,0;wf,21,1,1.

TABLE 5: Comparison of Experimental and Calculated VDEs in EV for B_3^-

experimental spectrum		theoretical spectrum			
			VDE		
band	VDE	final state	ROVGF/ 6-311+G(2df)[a]	ADC(3)/ 6-311+G(2df)	RCCSD(T)/ 6-311+G(2df)
X	2.82 ± 0.02	$^2A_1'$, $1a_1'^2 1e'^4 1a_2''^2 2a_1'^1$ $2e'^0$	2.72 (0.87)	2.68 (0.84)	2.88
A	3.56 ± 0.03	$^2A_2''$, $1a_1'^2 1e'^4 1a_2''^1 2a_1'^2$ $2e'^0$	3.57 (0.88)	3.57 (0.87)	3.54
B	4.55 ± 0.03	$^2E'$, $1a_1'^2 1e'^4 1a_2''^2 2a_1'^0$ $2e'^1$			4.70
		$^4E''$, $1a_1'^2 1e'^4 1a_2''^2 2a_1'^1$ $2e'^1$			4.82
C	5.58 ± 0.03	$^2E'$, $1a_1'^2 1e'^3 1a_2''^2 2a_1'^2$ $2e'^0$	5.31 (0.83)	5.43 (0.69)	

[a] Data from the ref 46.

photoelectron spectrum of the X peak suggested that there should be very little geometry change between the ground states of the anion and the neutral. Indeed, we only found a very slight elongation in the B−B bond length upon electron detachment (Table 2). The vibrational frequencies determined from the spectrum of the X band for B_3^- (1230 ± 40 cm^{-1}) and B_3 (1020 ± 50 cm^{-1}) are also in good agreement with the calculated totally symmetric stretching frequencies for B_3^- [$\omega_1(a_1) = 1239$ cm^{-1}] and B_3 [$\omega_1(a_1) = 1223$ cm^{-1}] at the B3LYP level (Table 2). The reduced vibrational frequency upon electron detachment suggests the bonding nature of the $2a_1'$ HOMO.

The next band (A) in the spectrum should correspond to detachment from the $1a_2''$ HOMO − 1, which is a π orbital delocalized throughout the B_3^- anion (Figure 5). For the A band, the calculated VDE at all three levels of theory is in excellent agreement with the experiment (Table 5).

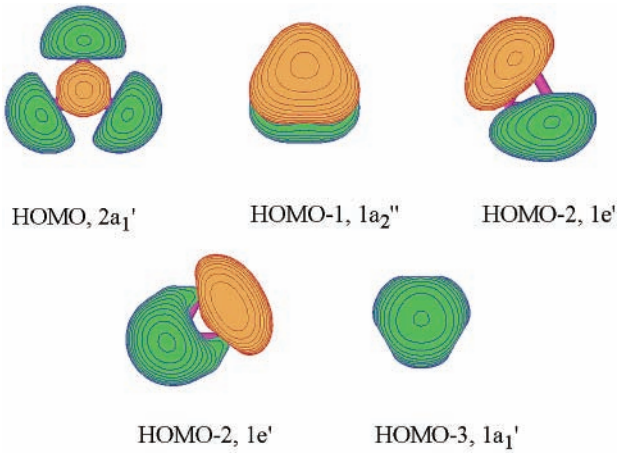

Figure 5. Occupied valence molecular orbitals of B_3^- (D_{3h}, $^1A_1'$).

6.2. B Band: Two-Electron Transitions. According to the ROVGF and ADC(3) calculations, there are no one-electron detachment processes between 3.6 and 5.3 eV. Yet, a relatively intense detachment band (B) was observed at 4.55 eV in the 193 nm spectrum (Figure 1c). This band was broad and exhibited a strong dependence on photon energies because it had negligible intensity in the 266 nm spectrum (Figure 1b). This peak could have several sources: (1) impurity, (2) isomer, (3) excited anion, and (4) multielectron transitions (shake-up). The first three causes could be ruled out immediately because more than one band would be expected for any of these three sources. Thus, B band could be only due to a multielectron process, i.e., a direct photodetachment accompanied by an electronic excitation in the final state.

We calculated two such transitions corresponding to two final electronic configurations $1a_1'^2 1e'^4 1a_2''^2 2a_1'^0$ $2e'^1$ (VDE = 4.70 eV) and $1a_1'^2 1e'^4 1a_2''^1 2a_1'^1$ $2e'^1$ (VDE = 4.82 eV) at the RCCSD(T)/6-311+G(2df) level of theory. The first transition corresponds to a two-electron process in which one electron was detached from the $2a_1'$-HOMO and a second electron was simultaneously excited from the $2a_1'$-HOMO into the $2e'$-LUMO. The calculated VDE (4.70 eV, Table 5) for this transition agrees well with the experimentally observed band B. The second transition corresponds again to a two-electron transition in which one electron was detached from the $1a_2''$-HOMO-1 and a second electron was simultaneously excited from the $2a_1'$-HOMO into the $2e'$-LUMO. The calculated VDE (4.82 eV, Table 5) for this transition is only higher than the first process by 0.12 eV and is also in the right energy range

TABLE 6: Comparison of the Experimental VDEs of B_4^- with Calculated VDEs for the $^2B_{1u}$ and ^2A_g States of B_4^-[a]

experimental spectra		theoretical interpretation		
			VDE	
band	VDE	final state	RCCSD(T)/ 6-311+G(2df)	EOM-RCCSD(T)/ 6-311+G(2df)
		$^2B_{1u}$ B_4^-		
X	1.99 ± 0.05	^1A_g, $1a_g^2 1b_{1u}^2 1b_{2u}^2 1b_{3u}^2 2a_g^2 1b_{3g}^2 2b_{1u}^0$	1.85[b]	
A	3.08 ± 0.03	$^3B_{2u}$, $1a_g^2 1b_{1u}^2 1b_{2u}^2 1b_{3u}^2 2a_g^2 1b_{3g}^1 2b_{1u}^1$	3.14	
B	3.41 ± 0.03	$^3B_{1u}$, $1a_g^2 1b_{1u}^2 1b_{2u}^2 1b_{3u}^2 2a_g^1 1b_{3g}^2 2b_{1u}^1$	3.24	
C	4.39 ± 0.05	$^1B_{2u}$, $1a_g^2 1b_{1u}^2 1b_{2u}^2 1b_{3u}^2 2a_g^2 1b_{3g}^1 2b_{1u}^1$		4.03
		$^3B_{2g}$, $1a_g^2 1b_{1u}^2 1b_{2u}^2 1b_{3u}^1 2a_g^2 1b_{3g}^2 2b_{1u}^1$	4.35	
		$^1B_{2g}$, $1a_g^2 1b_{1u}^2 1b_{2u}^2 1b_{3u}^1 2a_g^2 1b_{3g}^2 2b_{1u}^1$		4.65
		$^1B_{1u}$, $1a_g^2 1b_{1u}^2 1b_{2u}^2 1b_{3u}^2 2a_g^1 1b_{3g}^2 2b_{1u}^1$		5.37
		^2A_g B_4^-		
X	1.99 ± 0.05	^1A_g, $1a_g^2 1b_{1u}^2 1b_{2u}^2 1b_{3u}^2 1b_{3g}^2 2a_g^2 3a_g^0$	1.87[c]	
A	3.08 ± 0.03			
B	3.41 ± 0.03	^3A_g, $1a_g^2 1b_{1u}^2 1b_{2u}^2 1b_{3u}^2 1b_{3g}^2 2a_g^1 3a_g^1$	3.47	
		$^3B_{3g}$, $1a_g^2 1b_{1u}^2 1b_{2u}^2 1b_{3u}^2 1b_{3g}^1 2a_g^2 3a_g^1$	3.61	
C	4.39 ± 0.05	$^3B_{3u}$, $1a_g^2 1b_{1u}^2 1b_{2u}^2 1b_{3u}^1 1b_{3g}^2 2a_g^2 3a_g^1$	4.05	
		$^1B_{3g}$, $1a_g^2 1b_{1u}^2 1b_{2u}^2 1b_{3u}^2 1b_{3g}^1 2a_g^2 3a_g^1$		4.34
		$^1B_{3u}$, $1a_g^2 1b_{1u}^2 1b_{2u}^2 1b_{3u}^1 1b_{3g}^2 2a_g^2 3a_g^1$		4.57
		^1A_g, $1a_g^2 1b_{1u}^2 1b_{2u}^2 1b_{3u}^2 1b_{3g}^2 2a_g^1 3a_g^1$		4.61

[a] All energies are in eV. [b] VDE for this detachment process has been also calculated as an attachment to the $2b_{1u}$-LUMO of the neutral B_4 cluster using ROVGF/6-311+G(2df) and ADC(3)/6-311+G(2df) methods at the optimal RCCSD(T)/6-311+G* geometry of the $^2B_{1u}$ isomer. Calculated VDE was found to be 1.74 eV (ROVGF) and 2.07 eV (ADC(3)). [c] VDE for this detachment process has been also calculated as an attachment to the $3a_g$-LUMO of the neutral B_4 cluster using ROVGF/6-311+G(2df) and ADC(3)/6-311+G(2df) methods at the optimal RCCSD(T)/6-311+G* geometry of the ^2A_g isomer. Calculated VDE was found to be 1.55 eV (ROVGF) and 1.73 eV (ADC(3)).

for the B band. Therefore, the B band can be reliably assigned to be due to the two-electron transitions, which are manifestations of electron correlation effects in B_3^-. The relatively high intensity of the B band is surprising, indicative of unusually strong electron correlation effects in the boron trimer.

6.3. C Band. The highest binding energy feature observed in the 193 nm spectrum of B_3^- (Figure 1c) is the C band at 5.58 eV. According to the ROVGF and ADC(3) results (Table 5), this band corresponds to an electron detachment from the doubly degenerate HOMO-2 (1e′), which are composed primarily of 2s orbitals from the three boron atoms with some mixing from the 2p orbitals (Figure 5). The theoretical ROVGF and ACD(3) VDEs are in good agreement with the measured VDE for the C band. Electron detachment from the 1e′ orbitals results in a degenerate final state (^{2}E′), which is subject to Jahn−Teller distortions. However, the C band was relatively sharp with a discernible splitting (∼1100 cm^{-1}), suggesting the Jahn−Teller effect is weak or negligible. The 1100 cm^{-1} splitting was most likely due to a vibrational structure.

7. Interpretation of the Photoelectron Spectra of B_4^-

Even though the $^2B_{1u}$ state was calculated to be the ground state of B_4^- at B3LYP and CASSCF-MRCISD in the current study, RCCSD(T) gave the ^2A_g state to be the ground state (Table 4). Therefore, we calculated the theoretical VDEs from both states of B_4^-, as given and compared with the experimental data in Table 6. The MO pictures of B_4 and the two anionic isomers are shown in Figure 6 and will be used together with the VDEs to interpret the observed photoelectron spectra and help distinguish between the two anionic isomers.

7.1. B_4^- ($^2B_{1u}$). The first band (X) corresponds to detachment of an electron from the $2b_{1u}$-HOMO of B_4^-, which is depicted in Figure 6b. This transition yields the ground electronic state D_{2h} (^1A_g) for neutral B_4. There is a large geometry change between the $^2B_{1u}$ state of B_4^- and the ^1A_g ground state of B_4, primarily in their bond angles (see Tables 3 and 4). This large geometry change is in excellent agreement with the broad X band observed in the photoelectron spectrum of B_4^- (Figure 2). Good agreement was also found between the experimental VDE (1.99 ± 0.05 eV) and the corresponding to theoretical values (1.85 eV, Table 6). The first VDE can also be calculated as an electron attachment to neutral B_4 at the optimal geometry of the $^2B_{1u}$ B_4^-. The ADC(3) value (2.07 eV, see footnote a of Table 6) obtained using this procedure is in excellent agreement with the experimental value. The calculated ADE (1.60 eV) at RCCSD(T) is also in good agreement with the experimentally estimated value (∼1.6 eV).

The next three major detachment channels correspond to the removal of an electron from the $1b_{3g}$-HOMO-1, $2a_g$-HOMO-2, and $1b_{3u}$-HOMO-3 (Figure 6b), all yielding triplet final states. The calculated VDEs for these three channels are in excellent agreement with the experimental observations for the major bands A, B, and C (Table 6). A singlet final state can also be produced from each of these three detachment channels in one-electron transitions and should be observed in the photoelectron spectra although the intensities of the singlet states were expected to be lower than those of the triplet states. Using the EOM-RCCSD(T) method, we found that the three singlet states are within the energy range of the experiment at VDEs between 4.03 and 5.37 eV. The VDEs for the $^1B_{2u}$ and $^1B_{2g}$ states are in the vicinity of the C band, which was broad and should contain contributions from these two singlet states. The VDE of the $^1B_{1u}$ state (5.37 eV) is relatively high and falls in the high binding energy side of the 193 nm spectrum (Figure 2c), where there were weak detachment signals, though no distinct peak. Thus, an excellent agreement was observed between the theoretical results from the $^2B_{1u}$ ground state of B_4^- and the experimental photoelectron spectra of B_4^- both in the overall spectral pattern and the VDEs.

7.2. B_4^- (^2A_g). For the ^2A_g B_4^- state, the first detachment channel is from the $3a_g$-HOMO, which is depicted in Figure 6c. This transition yields the same ground electronic state D_{2h} (^1A_g) for B_4 (Table 3). Because at the RCCSD(T)/6-311+G-(2df) level of theory the ^2A_g and $^2B_{1u}$ states of B_4^- are almost

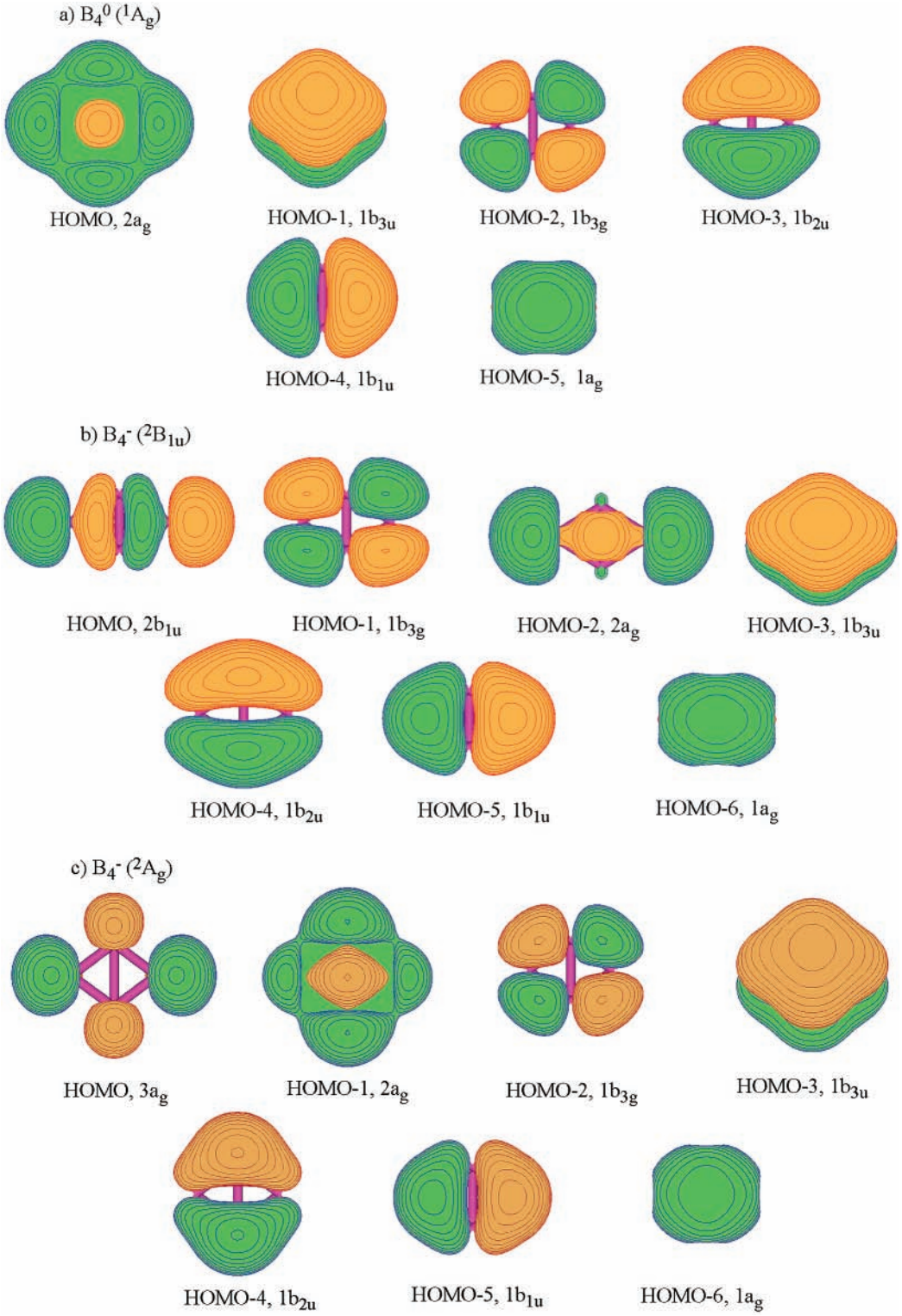

Figure 6. Occupied valence molecular orbitals of (a) B_4 (D_{2h}, ^1A_g), (b) B_4^- (D_{2h}, $^2B_{1u}$), and (c) B_4^- (D_{2h}, ^2A_g).

degenerate, an almost identical theoretical VDE was obtained from both anionic states. However, the first VDE evaluated using the electron attachment procedure is much lower than the experimental VDE (see footnote b of Table 6). Furthermore, there is little geometry change between the ^2A_g state of B_4^- and the ^1A_g ground state of B_4 (Tables 3 and 4). The bond angles are almost the same in the two states, except that the B−B bond lengths in B_4 are slightly shortened. Therefore, a very sharp photoelectron band would be expected from the ^2A_g B_4^- to the ^1A_g B_4 ground state with perhaps a short vibrational progression in the high frequency totally symmetric mode, which would have been easily resolved even under the lower resolution conditions. This expectation is clearly inconsistent with the observed broad spectra for the X band of B_4^- (Figure 2).

According to the RCCSD(T)/6-311+G(2df) calculations, there is no one-electron transition between 1.87 and 3.47 eV and the next three major detachment channels are from the $2a_g$-HOMO-1, $1b_{3g}$-HOMO-2, and $1b_{3u}$-HOMO-3 (Figure 6c), yielding VDEs of 3.47, 3.61, and 4.05 eV (Table 6), respectively, for the three triplet final states. This computed spectral

pattern disagrees completely with the three main detachment bands (A, B, and C) observed in the 193 nm spectrum of B_4^- (Figure 2c).

There are also three transitions into the singlet final states calculated to be between 4.34 and 4.61 eV (Table 6), which are in the same energy range of the C band, but cannot account for the intense C band in the experimental spectrum because their respective triplet states do not agree with the experimental spectrum.

Thus, we can rule out the ^2A_g state as a major contributor to the photoelectron spectra of B_4^-. The observed spectra should be primarily due to the $^2B_{1u}$ B_4^-, which was shown to be the ground state at the highest level of theory (Table 4).

8. Chemical Bonding in B_3^-, B_4, and B_4^-

8.1. B_3^-. Chemical bonding in the B_3^- anion was discussed before.[46] Here we briefly summarize the major conclusions from the previous work in order to relate to the B_4^- anion in the following discussion. As shown in Figure 5, of the five valence molecular orbitals, the $1a_1'$-HOMO-3 and $1e'$-HOMO-2 are formed primarily by the 2s orbitals of the boron atoms with some hybridization of the p orbital in the $1e'$-HOMO-2. Because all bonding, nonbonding, and antibonding MOs composed of the same type of atomic orbitals are occupied, the net bonding effect from these MOs should be small. Some contribution to the bonding from these three MOs may come from the s−p hybridization, but we expect this contribution to be small. The $1a_2''$-HOMO-1 is a bonding π orbital formed by the p_π orbitals of the three boron atoms. This MO is similar to the π orbital in the cyclopropyl cation ($C_3H_3^+$), thus rendering π aromaticity for the B_3^- anion.[46] The HOMO of B_3^- is a σ orbital formed by the p_σ-radial orbitals of the three boron atoms and is a bonding MO contributing to the stability of B_3^-. The two π electrons obey the $(4n + 2)$ Huckel rule for aromaticity for the $n = 0$ case. The $2a_1'$ σ-bonding MO is also completely delocalized among the three boron atoms, giving the characteristic of σ aromaticity for B_3^-. Thus, the B_3^- anion is both π and σ aromatic, i.e., doubly aromatic. The aromatic nature of the HOMO and HOMO − 1 is also confirmed by their rather high VDEs (Table 5).

8.2. B_4. Before considering the chemical bonding in B_4^-, let us first discuss the B_4 neutral cluster. Neutral B_4 has an unexpected valence electronic configuration $1a_g^2 1b_{1u}^2 1b_{2u}^2 1b_{3g}^2 1b_{3u}^2 2a_g^2$, and the corresponding MO pictures are presented in Figure 6a. Usually, we expected that all four MOs composed primarily of the 2s orbitals of the boron atoms to be occupied first before MOs composed of the 2p orbitals of boron, as is the case in B_3^- (Figure 5) or more thoroughly discussed in Al_4^{2-}.[75−77] Yet, we found that one of the four 2s-based MOs, the antibonding combination of the 2s orbitals of boron (the HOMO in Figure 6c), is actually unoccupied. The $2a_g$-HOMO of B_4 is a completely bonding σ orbital formed by the $2p_\sigma$-radial orbitals of the four boron atoms. The $1b_{3u}$-HOMO − 1 is a completely bonding π-molecular orbital formed by the $2p_\pi$ orbitals of boron and the $1b_{3g}$-HOMO − 2 is a completely bonding σ MO formed by the $2p_\sigma$-perpendicular orbitals of boron. As previously discussed for Al_4^{2-}, we can identify three types of molecular orbitals formed by the three types of 2p orbitals ($p_{x,y,z}$) of boron: (1) $2p_z$ or $2p_\pi$ atomic orbital, (2) $2p_x$ or $2p_{\sigma-r}$ atomic orbital (σ-radial orbital oriented toward the center of the cluster), and (3) $2p_y$ or $2p_{\sigma-p}$ (σ-perpendicular orbital oriented perpendicular to the radial orbital). The three sets of atomic orbital ($2p_\pi$, $2p_{\sigma-r}$, and $2p_{\sigma-p}$) from the four boron atoms each form a set of molecular orbitals with the lowest MO being completely bonding, the next two doubly degenerate MOs being bonding/antibonding (or nonbonding), and the highest MO completely antibonding. On the basis of these three sets of MOs, we can introduce three types of aromaticity according to the delocalization patterns of the MOs: the π aromaticity due to the MOs formed by the $2p_\pi$ atomic orbitals and two types of σ aromaticity due to the MOs formed by either the $2p_{\sigma-r}$ or the $2p_{\sigma-p}$ atomic orbitals. The lowest three occupied MOs (Figure 6a), the $1b_{2u}$-HOMO-3, $1b_{1u}$-HOMO-4, and $1a_g$-HOMO-5, are primarily boron 2s orbitals with an appreciable contribution from 2p-orbitals.

The three highest occupied MOs of B_4 are the three lowest bonding MOs from each of the three types atomic orbitals discussed above. This MO pattern is nearly identical to that in Al_4^{2-},[75−77] making neutral B_4 triply aromatic, i.e., π aromatic and doubly σ aromatic, analogous to that in Al_4^{2-}. That this is possible in B_4, which has two fewer electrons than Al_4^{2-}, is because of the fact that one of the 2s-MOs in B_4 is not occupied. As discussed previously,[75−77] the presence of the delocalized π and σ MOs in Al_4^{2-} is responsible for its square-planar structure.

However, the question is why B_4, with the same set of occupied aromatic orbitals as Al_4^{2-}, does not possess a perfect square structure. We suspect that this is caused by the fact that the 2s antibonding MO in B_4 is unoccupied, such that the three occupied 2s lone pairs must be shared among the four atoms. Examining the three occupied 2s MOs of B_4, we found a significant s−p hybridization, in contrast to Al_4^{2-}, where the 3s MOs are pure lone pairs with very little mixing with the 3p orbitals. This is understandable because the 2s and 2p orbitals are much closer in energy than the 3s and 3p orbital in Al. Furthermore, the B−B bond length (1.558 Å) in B_4 is much shorter than the Al−Al bond length (2.58 Å) in Al_4^{2-},[75−77] indicating much stronger bonding in the boron cluster. However, even though the neutral B_4 cluster is slightly rhombus, it is still a highly aromatic system, as was recently confirmed using nuclear-independent chemical shift.[34] As a matter of fact, the distortion from a perfect square in B_4 is quite small. At the B3LYP level of theory (Figure 4), the D_{4h} structure (XI), which is a transition state, is only 0.81 kcal/mol higher than the D_{2h} ground state. If the zero-point energies are taken into account, this energy difference is even smaller. Thus, the potential energy surface along the rhombus distortion is quite flat, as confirmed by the very low vibrational frequency of the $\omega_2(a_g)$ mode (Table 3).

8.3. B_4^-. The two $^2B_{1u}$ and ^2A_g isomers of B_4^- have the same ($1a_g^2 1b_{1u}^2 1b_{2u}^2 1b_{3g}^2 1b_{3u}^2 2a_g^2$) core of closed shell MOs as in neutral B_4, but the extra electron enters different MOs (Figure 6, parts b and c). In B_4^- (^2A_g), the extra electron occupies the $3a_g$-HOMO, which is the 2s lone pair antibonding MO. This MO is very low-lying in Al_4^{2-},[75−77] but is pushed up in neutral B_4. Upon further occupation of this MO by a second electron, the B_4^{2-} dianion acquires the same valence electronic configuration as the Al_4^{2-} dianion[75−77] and does become a perfect square. In B_4^- ($^2B_{1u}$), the extra electron enters the $2b_{1u}$-HOMO, which is an bonding/antibonding MO composed of p_σ orbitals from the two apex boron atoms (B2 and B4 in structure I, Figure 3). The antibonding nature of the $2b_{1u}$ MO pushes apart the atoms B2 and B4, significantly reducing the ∠B1−B2−B3 bond angle. However, this rhombus distortion enhances the bonding interaction between B1 and B3. The net gain of the B1−B3 bonding in the $^2B_{1u}$ B_4^- is why this isomer is slightly more favored than the ^2A_g state.

The $^2B_{1u}$ structure is still π-aromatic because of the presence of the $1b_{3u}$ HOMO − 3. The $1b_{3g}$ HOMO − 1 is a σ-aromatic

orbital, similar to that in neutral B_4 (Figure 5). The $2b_{1u}$ HOMO and $2a_g$ HOMO − 2 are antibonding and bonding combinations of the $p_{\sigma-r}$ orbitals on B2 and B4 and make the B_4^- cluster σ-antiaromatic, despite the presence of the σ-aromatic $1b_{3g}$ orbital. The rhombus distortion can be viewed as a consequence of the σ-antiaromaticity, analogous to the rectangular distortion in cyclobutadiene or Al_4^{4-} due to the π antiaromaticity.[78] The antibonding (antiaromatic) nature of the $2b_{1u}$ HOMO is confirmed by its appreciably low VDE (1.99 eV). The bonding $2a_g$ HOMO − 2, as well as the two aromatic MOs ($1b_{3g}$ and $1b_{3u}$), all have substantially higher VDEs.

9. Conclusions

The electronic and geometrical structures and chemical bonding of the two smallest boron clusters, the trimer and tetramer, in the neutral and anionic forms were investigated using photoelectron spectroscopy and ab initio calculations. Well resolved photoelectron spectra were obtained for B_3^- and B_4^- at various photon energies, providing experimental electronic structure and vibrational information. We confirmed that both B_3^- and B_3 have D_{3h} symmetry with doubly (σ and π) aromatic characteristics. An unusually intense peak due to two-electron transitions was observed in the 193 nm spectrum of B_3^- and was characterized theoretically, suggesting strong electron correlation effects in the boron trimer.

The neutral B_4 cluster is slightly distorted from a perfect square structure but still possesses doubly σ aromaticity and π aromaticity. For B_4^-, we identified two low-lying isomers with rhombus shapes, D_{2h} $^2B_{1u}$ and D_{2h} ^2A_g. The D_{2h} $^2B_{1u}$ isomer has a significant distortion from the perfect square structure with a 64° ∠B1−B2−B3 angle, whereas the D_{2h} ^2A_g isomer has a relatively small distortion from the perfect square structure with a 74° ∠B1−B2−B3 angle. Our calculations suggest that the D_{2h} ($^2B_{1u}$) isomer is slightly more stable than the D_{2h} (^2A_g) isomer. The D_{2h} ($^2B_{1u}$) isomer as the ground state of B_4^- was confirmed by the excellent agreement between the calculated VDEs with the experimental data. Molecular orbital analyses revealed that the D_{2h} ($^2B_{1u}$) B_4^- is π-aromatic but σ antiaromatic that causes the rhombus distortion.

Acknowledgment. The theoretical work done at Utah was supported by the donors of the Petroleum Research Fund (ACS-PRF# 38242-AC6), administered by the American Chemical Society. The experimental work done at Washington was supported by the National Science Foundation (DMR-0095828) and performed at the W. R. Wiley Environmental Molecular Sciences Laboratory, a national scientific user facility sponsored by DOEs Office of Biological and Environmental Research and located at Pacific Northwest National Laboratory, which is operated for DOE by Battelle.

References and Notes

(1) Cotton, F. A.; Wilkinson, G.; Murillo, C. A.; Bochmann, M. *Advanced Inorganic Chemistry*, 6th ed.; John Wiley & Sons: New York, 1999.
(2) Greenwood, N. N.; Earnshaw, A. *Chemistry of Elements*, 2nd ed.; Buttwerworth-Heinemann: Oxford, U.K., 1997.
(3) Tang, A. C.; Li, Q. S. *Int. J. Quantum Chem.* **1986**, *29*, 579.
(4) Hanley, L.; Whitten, J. L.; Anderson, S. L. *J. Phys. Chem.* **1988**, *92*, 5803.
(5) Martin, J. M. L.; Francois, J. P.; Gijbels, R. *J. Chem. Phys.* **1989**, *90*, 6469.
(6) Hernandez, R.; Simons, J. *J. Chem. Phys.* **1991**, *94*, 2961.
(7) Kato, A. U.; Tanaka, E. *J. Comput. Chem.* **1991**, *12*, 1097.
(8) Kato. A. U.; Yamashita. K.; Morokuma. K. *Chem. Phys. Lett.* **1992**, *190*, 361.
(9) Martin, J. M. L.; Francois, J. P.; Gijbels, R. *Chem. Phys. Lett.* **1992**, *189*, 529.
(10) Kawai, R.; Weare, J. H. *Chem. Phys. Lett.* **1992**, *191*, 311.
(11) Ray, A. K.; Howard, I. A.; Kanal, K. M. *Phys. Rev. B* **1992**, *45*, 14247.
(12) Hernandez, R.; Jorgenson, P.; Simons, J. *J. Chem. Phys.* **1993**, *98*, 3060.
(13) Boustani, I. *Int. J. Quantum Chem.* **1994**, *52*, 1081.
(14) Meden, A.; Mavri, J.; Bele, M.; Pejovnik, S. *J. Phys. Chem.* **1995**, *99*, 4252.
(15) Boustani, I. *Chem. Phys. Lett.* **1995**, *233*, 273.
(16) Boustani, I. *Chem. Phys. Lett.* **1995**, *240*, 135.
(17) Boustani, I. *Surf. Sci.* **1996**, *370*, 355.
(18) Ricca, A.; Bauschlicher, C. W. *Chem. Phys.* **1996**, *208*, 233.
(19) Ricca, A.; Bauschlicher, C. W. *J. Chem. Phys.* **1997**, *106*, 2317.
(20) Niu, J.; Rao, B. K.; Jena, P. *J. Chem. Phys.* **1997**, *107*, 132.
(21) Boustani, I. *Phys. Rev. B* **1997**, *55*, 16426.
(22) Gu, F. L.; Yang, X. M.; Tang, A. C.; Jiao, H. J.; Schleyer, P. v. R. *J. Comput. Chem.* **1998**, *19*, 203.
(23) Boustani, I.; Quandt, A. *Comput. Mater. Sci.* **1998**, *11*, 132.
(24) Boustani, I.; Rubio, A.; Alonso, J. A. *Chem. Phys. Lett.* **1999**, *311*, 21.
(25) McKee, M. L.; Wang, Z. X.; Schleyer, P. v. R. *J. Am. Chem. Soc.* **2000**, *122*, 4781.
(26) Fowler, J. E.; Ugalde, J. M. *J. Phys. Chem. A* **2000**, *104*, 397.
(27) Aihara, J. *J. Phys. Chem. A* **2001**, *105*, 5486.
(28) Cao, P.; Zhao, W.; Li, B.; Song, B.; Zhou, X. *J. Phys.: Condens. Matter*. **2001**, *13*, 5065.
(29) Petters, A.; Alsenoy, C. V.; March, N. H.; Klein, D. J.; Van Doren, V. E. *J. Phys. Chem. B* **2001**, *105*, 10546.
(30) Luo, W.; Clancy, P. *J. Appl. Phys.* **2001**, *89*, 1596.
(31) Li, Q. S.; Jin, H. W. *J. Phys. Chem. A* **2002**, *106*, 7042.
(32) Ma, J.; Li, Z.; Fan, K.; Zhou, M.; *Chem. Phys. Lett.* **2003**, *372*, 708.
(33) Havenith, R. W. A.; Fowler, P. W.; Steiner, E. *Chem. Eur. J.* **2002**, *8*, 1068.
(34) Jin, H. W.; Li, Q. S. *Phys. Chem. Chem. Phys.* **2003**, *5*, 1110.
(35) Zhai, H. J.; Wang, L. S.; Alexandrova, A. N.; Boldyrev, A. I. *J. Chem. Phys.* **2002**, *117*, 7917.
(36) Alexandrova, A. N.; Boldyrev, A. I.; Zhai, H. J.; Wang, L. S.; Heiner, E.; Fowler, P. W. *J. Phys. Chem. A* **2003**, *107*, 1359.
(37) Zhai, H. J.; Wang, L. S.; Alexandrova, A. N.; Boldyrev, A. I. *Angew. Chem. Int. Ed.* in press.
(38) Zhai, H. J.; Kiran, B.; Li, J.; Wang, L. S. To be published.
(39) Hanley, L.; Anderson, S. L. *J. Phys. Chem.* **1987**, *91*, 5161.
(40) Hintz, P. A.; Ruatta, S. A.; Anderson, S. L. *J. Chem. Phys.* **1990**, *92*, 292.
(41) Ruatta, S. A.; Hintz, P. A.; Anderson, S. L. *J. Chem. Phys.* **1991**, *94*, 2833.
(42) Hintz, P. A.; Sowa, M. B.; Ruatta, S. A.; Anderson, S. L. *J. Chem. Phys.* **1991**, *94*, 6446.
(43) Placa, S. J.; La Roland, P. A.; Wynne, J. J. *Chem. Phys. Lett.* **1992**, *190*, 163.
(44) Harmick, Y. M.; Van Zee, R. J.; Weltner, W., Jr. *J. Chem. Phys.* **1992**, *96*, 1767.
(45) Sowa-Resat, M. B.; Smolanoff, J.; Lapiki, A.; Anderson, S. L. *J. Chem. Phys.* **1997**, *106*, 9511.
(46) Kuznetsov, A. E.; Boldyrev, A. I. *Struct. Chem.* **2002**, *13*, 2.
(47) Wang, L. S.; Cheng, H. S.; Fan, J. *J. Chem. Phys.* **1995**, *102*, 9480.
(48) Wang, L. S.; Wu, H. in *Advances in Metal and Semiconductor Clusters. IV. Cluster Materials*; Duncan, M. A., Ed.; JAI Press: Greenwich, 1998; p 299.
(49) Parr, R. G.; Yang, W. *Density-functional theory of atoms and molecules*; Oxford University Press: Oxford, U.K., 1989.
(50) Becke, A. D. *J. Chem. Phys.* **1993**, *98*, 5648.
(51) Perdew, J. P.; Chevary, J. A.; Vosko, S. H.; Jackson, K. A.; Pederson, M. R.; Singh, D. J.; Fiolhais, C. *Phys. Rev. B* **1992**, *46*, 6671.
(52) McLean, A. D.; Chandler, G. S. *J. Chem. Phys.* **1980**, *72*, 5639.
(53) Clark, T.; Chandrasekhar, J.; Spitznagel, G. W.; Schleyer, P. v. R. *J. Comput. Chem.* **1983**, *4*, 294.
(54) Frisch, M. J.; Pople J. A.; Binkley, J. S. *J. Chem. Phys.* **1984**, *80*, 3265.
(55) Cizek, J. *Adv. Chem. Phys.* **1969**, *14*, 35.
(56) Knowles, P. J.; Hampel, C.; Werner, H.-J. *J. Chem. Phys.* **1993**, *99*, 5219.
(57) Raghavachari, K.; Trucks, G. W.; Pople, J. A.; Head-Gordon, M. *Chem. Phys. Lett.* **1989**, *157*, 479.
(58) Bernardi, F.; Bottini, A.; McDougall, J. J. W.; Robb, M. A.; Schlegel, H. B. *Faraday Symp. Chem. Soc.* **1979**, *19*, 137.
(59) Frisch, M. J.; Ragazos, I. N.; Robb, M. A.; Schlegel, H. B. *Chem. Phys. Lett.* **1992**, *189*, 524.
(60) Werner, H.-J.; Knowles, P. J. *J. Chem. Phys.* **1988**, *89*, 5803.
(61) Knowles, P. J.; Werner, H.-J. *Chem. Phys. Lett.* **1988**, *145*, 514.

(62) Schirmer, J.; Cederbaum, L. S.; Walter, O. *Phys. Rev. A* **1983**, *28*, 1237.
(63) von Niessen, W.; Schirmer, J.; Cederbaum, L. S. *Comput. Phys. Rep*. **1984**, *1*, 57.
(64) Schirmer, J.; Angonoa, G. *J. Chem. Phys.* **1989**, *91*, 1754.
(65) Ortiz, J. V. *J. Chem. Phys.* **1998**, *108*, 1008.
(66) Zakrzewski, V. G.; Dolgounitcheva, O.; Ortiz, J. V. *Int. J. Quantum Chem*. **1999**, *75*, 607.
(67) Stanton, J. F.; Bartlett, R. J. *J. Chem. Phys.* **1993**, *99*, 7029 and references therein.
(68) Cederbaum, L. S. *J. Phys. B* **1975**, *8*, 290.
(69) Zakrzewski, V. G.; von Niessen, W. *J. Comput. Chem.* **1993**, *14*, 13.
(70) Zakrzewski, V. G.; Ortiz, J. V. *Int. J. Quantum Chem.* **1995**, *53*, 583.
(71) For a recent review, see: Ortiz, J. V.; Zakrzewski, V. G.; Dolgunitcheva, O. *Conceptual Trends Quantum Chem.* **1997**, *3*, 463.
(72) Frisch, M. J.; Trucks, G. W.; Schlegel, H. B.; Scuseria, G. E.; Robb, M. A.; Cheeseman, J. R.; Zakrzewski, V. G.; Montgomery, J. A., Jr.; Stratmann, R. E.; Burant, J. C.; Dapprich, S.; Millam, J. M.; Daniels, A. D.; Kudin, K. N.; Strain, M. C.; Farkas, O.; Tomasi, J.; Barone, V.; Cossi, M.; Cammi, R.; Mennucci, B.; Pomelli, C.; Adamo, C.; Clifford, S.; Ochterski, J.; Petersson, G. A.; Ayala, P. Y.; Cui, Q.; Morokuma, K.; Malick, D. K.; Rabuck, A. D.; Raghavachari, K.; Foresman, J. B.; Cioslowski, J.; Ortiz, J. V.; Stefanov, B. B.; Liu, G.; Liashenko, A.; Piskorz, P.; Komaromi, I.; Gomperts, R.; Martin, R. L.; Fox, D. J.; Keith, T.; Al-Laham, M. A.; Peng, C. Y.; Nanayakkara, A.; Gonzalez, C.; Challacombe, M.; Gill, P. M. W.; Johnson, B. G.; Chen, W.; Wong, M. W.; Andres, J. L.; Head-Gordon, M.; Replogle, E. S.; Pople, J. A. *Gaussian 98*, revision A.7; Gaussian, Inc.: Pittsburgh, PA, 1998.
(73) Werner, H.-J.; Knowles, P. J.; with contributions from Amos R. D.; Bernhardsson A.; Berning, A.; Celani, P.; Cooper, D. L.; Deegan, M. J. O.; Dobbyn, A. J.; Eckert, F.; Hampel, C.; Hetzer, G.; Korona, T.; Lindh, R.; Llpyd, A. W.; McNicholas, S. J.; Manby, F. R.; Meyer, W.; Mura, M. E.; Nicklass, A.; Palmieri, P.; Pitzer, R.; Rauhut, G.; Schutz, M.; Stoll, H.; Stone, A. J.; Tarroni, R.; Thorsteinsson, T. *MOLPRO-1999*.
(74) MO pictures were made using the MOLDEN3.4 program. Schaftenaar, G. MOLDEN 3.4; CAOS/CAMM Center: The Netherlands, 1998.
(75) Li, X.; Kuznetsov, A. E.; Zhang, H.-F.; Boldyrev, A. I.; Wang, L. S. *Science* **2001**, *291*, 859.
(76) Kuznetsov, A. E.; Boldyrev, A. I.; Li, X.; Wang, L. S. *J. Am. Chem. Soc*. **2001**, *123*, 8825.
(77) Boldyrev, A. I.; Kuznetsov, A. E. *Inorg. Chem.* **2002**, *41*, 532.
(78) Kuznetsov, A. E.; Birch, K. A.; Boldyrev, A. I.; Li, X.; Zhai, H. J.; Wang, L. S. *Science* **2003**, *300*, 622.